Challenges and uncertainty in the seismic reservoir characterization of Bone Spring and Wolfcamp formations in the Delaware Basin using rock physics

Ritesh Kumar Sharma[†], Satinder Chopra[†], James Keay[‡] and Larry R. Lines[+]*

[†]TGS, Calgary; [‡]TGS, Houston; [+] University of Calgary, Canada

Summary

Amongst other things, rock physics analysis is usually carried out for estimating the volume of clay, water saturation and porosity using seismic data. Though these rock-physics parameters are easy to compute for conventional plays, there are a lot of uncertainties in their estimation for unconventional plays, especially where multizones need to be characterized simultaneously. We discuss them with reference to a dataset from the Delaware basin where the Bone Spring, Wolfcamp, Barnett and the Mississippian formations are the prospective zones. We elaborate on the challenges and the uncertainties in the characterization of these multi-zones, and how we overcome them. Our conclusion is that any deterministic approach (single rock-physics model) for characterization of the target formations of interest may not be appropriate and we build the case for adopting a robust statistical approach, comprising a graphical crossplot method and employing Bayesian classification. While the former makes use of neutron and density porosity data for defining the different lithofacies, the latter yields the uncertainty associated with the individual lithofacies. In this whole exercise, we begin with well-log data and define different lithofacies based on the graphical crossplot method. Thereafter, we correlate these facies with the interpreted mud-log data available for one well. Having gained the confidence in defining the different lithofacies, we then determine the lithofacies and their probabilities using the seismic impedance inversion attributes. The resultant facies seem convincing and correlate well with facies information derived from mud-log data interpretation.

Challenges and uncertainty in the characterization of shale formations using rock-physics analysis

Rock-physics analysis consists of two parts namely modeling and inversion. As the names suggest, attempts are first made to model the elastic response using mineral fractions, water saturations and porosity. Thereafter, rock-physics properties mentioned above are extracted using elastic properties computed using seismic impedance inversion.

As per rock physics, the elastic modulus (M) of a rock can be expressed as follows

$$\frac{1}{M} = \sum_i^n \frac{(1-\emptyset)V_i}{M_i} + \frac{\emptyset}{M_{fluid}}. \qquad (1)$$

where M_i are the i^{th} mineral moduli and V_i are the i^{th} mineral volume fraction.

As can be gauged from the equation above, parameters such as mineral volume fraction, water saturation and porosity play an important role in the rock-physics analysis. While these parameters are relatively easy to estimate for conventional reservoirs, there are a lot of uncertainties in their estimations for unconventional reservoirs. Some of the challenges are discussed below.

Uncertainty in the estimation of volume of shale from well-log data

Based on the fact that shale is usually more radioactive than sandstones and carbonates, the gamma-ray log curves are used to distinguish shale formations (with higher values) from others. Not only that, gamma-ray logs can also be used to determine the volume of shale present in a formation. Of course, there are other ways of computing the volume of shale from different well-log curves, but gamma-ray logs happen to be one of the methods, where first gamma-ray index is computed and is then transformed into volume of shale using linear or nonlinear empirical relationship. The gamma ray index is defined as $I_{GR}=(GR_{log}-GR_{min})/(GR_{max}-GR_{min})$; I_{GR} represents gamma-ray index, GR_{log} represents the gamma-ray reading at any depth, GR_{min} represents the minimum gamma-ray value which would correspond to clean sandstone, GR_{max} represents the maximum gamma-ray value which would correspond to shale. Thus, one needs at least one or more points on a clean sand, and similarly some points on a real shale rock in the shale interval under investigation. In the absence of such values, the computation could fall apart. For bringing in accuracy in such calculations, a linear correction through the use of a scalar multiplication has been suggested but results in an overestimation of V_{sh}. Empirical nonlinear corrections have been suggested by Larionov (1969), one for Tertiary or younger rocks, and another one for older rocks (Asquith and Krygowski, 2004). Some other corrections by Stieber (1970) and Clavier (1971) have also been proposed. All these corrections result in improved estimates in certain situations, but inaccuracies still show up in shaly sand formations. However, such empirical corrections have the drawback that they require other independent log curves or core data for calibration.

In order to capture the differences among different approaches we implement them on well-log data over a 3D seismic volume from Delaware Basin. In Figure 1, the sonic, density and gamma-ray curves from a well are shown in tracks 1, 2 and 3. The red curves show the input curves as such and the blue curves are their smoothed versions, which were used in the computations. In track 4, the computed volume of shale curve is shown in red, along with the scaled curve in blue and the curve with Stieber correction in black. Notice the large variations in these curves which will introduce discrepancies in the computations they are used in. The volume of shale was computed by a petrophysicist by first subdividing the curves into five basic zones, with the prominent ones being the Bone Spring, Wolfcamp and the Barnett/Mississippian intervals. Next, the minimum and maximum values of gamma-ray log in the respective zones were picked up. Finally, the computations of gamma-ray index were merged into a single composite curve, shown in track 5. This turns out to be different from the other curves shown in track 4.

Thus, we see there is uncertainty associated with the determination of volume of shale depending on the type of method adopted. The rule of thumb is to use minimum value of V_{sh} estimated using above approaches or the one which shows the maximum correlation with available XRD data.

10.1190/segam2019-3214084.1

Uncertainty in the determination of water saturation

Any well-log evaluation for estimation of water saturation in shales will depend on the type of shale and its volume. Usually the resistivity log is used to estimate the water saturation in the undisturbed formations of interest. As the resistivity in the matrix is high, any change in the measured resistivity comes from the fluid present in the pores of the formation. Archie's equation (Archie, 1952) is an empirical relationship that was derived for clean sandstones but works well for some nonclean formations also and is usually used to compute water saturation. Even though it remains flexible in its use, it needs to be modified for its application to shales and carbonates. For nonshaly rocks, it is a good idea to consider the volume of shale in the matrix to account for excess conductivity. The Simandoux equation (Simandoux, 1963) does that but it remains unclear which equation should be used to determine water saturation.

Uncertainty in the determination of porosity

In a given formation, if the bulk density (ρ_b) is known (from well-log data), and the density of the matrix (ρ_m) and the fluid (ρ_f) is also known, the porosity of that formation can be calculated as $\phi = (\rho_m - \rho_b)/(\rho_m - \rho_f)$. Usually, a constant value of matrix density (sandstone, limestone, dolomite) is used for porosity estimation in the above equation. Such an approach works well for conventional plays. Besides, in the Delaware Basin, the formations of interest (Bone Spring, Wolfcamp, Barnett) represent a series of multiple stacked transgressive sequences composed of naturally fractured, low-porosity interbedded carbonates, clastic sands, and shales. These formations are composed of varying amounts of quartz, calcite, dolomite, kerogen and clay minerals (illite, albite and pyrite). Such a mixture of minerals results in grain densities varying from 2.5 g/cm^3 to 2.7 g/cm^3 and pose a major challenge in the estimation of porosity, water-saturation and organic richness. An uncertainty range of 0.2 g/cm^3 can increase the error bar on porosity by 6%, which can drastically impact resource estimation (Malik et al., 2013).

Kim et al. (2016) also have shown the importance of matrix density in porosity determination in the Horn River Basin in Canada. In the presence of gas, the porosity calculated using the equation above results in a higher value for the reservoir when the density log data is used, as the density calculation itself is affected by the presence of gas. This calls for the use of a lower value of fluid density in the equation. Even when the ECS (elemental capture spectroscopy)-determined grain-density log is used, and if any value greater than zero is used for fluid density, the porosity computation using the above equation results in an overestimated value. This, therefore, questions the validity of the equation for the determination of porosity in the exercise at hand.

With the detailed descriptions given above for the challenges and the large uncertainties in the estimation of volume of shale, porosity and water saturation, an uncalibrated petrophysical/rock-physics model in the complex depositional environment of the Delaware Basin will lead to large uncertainties in the computed rock-physics properties. *The inherent implication in this conclusion is that any deterministic approach adopted for characterization of the target formations in the Delaware Basin may not be appropriate.* We therefore recommend that a statistical approach be considered for the purpose.

Following a statistical approach

In the Delaware Basin, the formations of interest (Bone Spring, Wolfcamp, Barnett) represent a series of multiple stacked transgressive sequences composed of naturally fractured, low-porosity interbedded carbonates, clastic sands, and shales. As stated above, these formations are composed of varying amounts of quartz, calcite, dolomite, kerogen and mainly clay minerals (illite, albite and pyrite). It would therefore help to understand the different types of facies, and how to identify them in the Delaware Basin. The *type, volume of shale* and *effective porosity* of a formation can be determined using well-log data with a *graphical crossplot method* as has been demonstrated by Ghorab et al. (2008) and Alaskari and Roozmeh (2017). The authors attempt to distinguish between laminated, dispersed and structural shale types amongst other applications.

The neutron-porosity (ϕ_N) and density-porosity (ϕ_D) data are crossplotted for the shale interval under investigation as shown in Figure 2. Three points are marked on this crossplot, namely, point F that represents fluid or water point, where $\phi_D = \phi_N = 100\%$, point M that represents matrix point where $\phi_D = \phi_N = 0$ (which will be true if the neutron and density tools are calibrated), and the shale point SH. The location of SH represents the shaliest segment of the well and will vary from one well to another. The porosity values on both axes do not exceed 0.5, as these are the maximum limit of porosity realizable. The well-data points from ϕ_D and ϕ_N curves entering the crossplot need to be corrected for the presence of hydrocarbons. On Figure 2, the well-data points from $\phi_D$and ϕ_N curves representing clean formations will fall along the line MF, and their location will indicate the effective porosity. Points along the line M-SH will have $\phi_e = 0$ and represent the volume of shale with zero effective porosity. Based on the characteristics of each of the shale types, the data points from the laminated shale will fall along or around the line LS-SH, the dispersed shale points along or around line DIS, and structural shale points along or around line STR. However, *in the absence of core samples and their descriptions, it may be difficult to confirm any such facies analysis that may be carried out*. Nevertheless, the above graphical method has helped us understand and describe the different facies that we assign to the different clusters in ϕ_D and ϕ_N crossplot space, which we describe in the next section.

Utilizing a robust statistical approach for characterization of unconventional plays

The ϕ_N and ϕ_D logs were picked up for five deep wells (W1-W5) covering our broad zone of interest, and crossplotted for the interval, Bone Spring to Woodford shale as shown in Figure 3. The cluster of data points are colour coded with resistivity. Two different trends, one corresponding to the carbonates and the other corresponding to the shales are seen on the crossplot. Based on the interpretation of Figure 2, the points close to the apex M and SH must be coming from limestone matrix and shaly formations respectively. Points along the clean carbonate formation line have been interpreted as tight limestone, moderate-quality limestone and high-quality limestone. Additionally, points along the line MSH have been interpreted as coming from shaly-limestone, limy-shale and clay-rich shale. Similarly, the points along line SH-LS are interpreted as coming from organic-rich shale. We confirm our observation that three different facies enclosed by the polygons in cyan, yellow and yellowish-green are representing the Bone Spring formation, which agrees with a similar conclusion arrived at by

10.1190/segam2019-3214084.1

Franseen et al. (2016). The clay-rich shale and the organic-rich shale facies seem to be coming from the Barnett to Mississippian interval. The shaly-limestone and limy-shale facies are observed within the Wolfcamp zone.

Next, we pulled out the mud-log interpretation available for one well and tried to seek out the facies for each of the individual intervals that we have interpreted. In Figure 4 we show how the well log-derived facies (siliceous mudstone) compares to the mud log interpretation. Favorable comparisons were noticed for all the well-defined facies which lent us confidence in the facies we had defined. As we are trying to characterize the different facies from well data between Bone Spring and Mississippian markers using different polygons, it is possible that a wide range of values within each polygon may represent the same facies. Understandably, the cluster points closer to the center within each polygon for the same facies should be more probable than the points away from the center. Consequently, we can follow an approach that accounts for the uncertainties associated with the different facies. This work follows the Bayesian classification approach and provides a facies model reflecting the quality of the lithounits and a related uncertainty analysis. For executing the Bayesian approach, the different facies were defined based on the cut off values of ϕ_D and ϕ_N well curves for the broad zone from Bone Spring to Mississippian. The eight facies as interpreted earlier, and their probability density function (PDF) are shown by the different colored ellipses in Figure 5a. Once this was done, the next question we tried to address was if it is possible to see such lithoclassification in the crossplot space of seismically derived attributes. For doing so, various combinations of parameters such as (P-impedance vs V_P/V_S, S-impedance vs rho, Lambda-rho vs Mu-rho, etc.) were considered. The commonly used crossplot of P-impedance vs V_P/V_S is shown in Figure 5b. Notice the excessive overlap and thus the complication of defining different facies in the elastic parameter domain. Thus, we conclude that the ϕ_N and ϕ_D are essential for the characterization of our zone of interest, and we need to derive them from seismic data. In most cases, as ϕ_D is derived from density data, it might be a good approach to compute the density attribute from seismic data first and then transform it into density porosity. The density estimation from seismic data requires either data with large offsets or multicomponent seismic data, and both these were not available. A neural-network approach (multiattribute regression analysis) is an alternative way for computation of density (Sharma et al., 2018). In this exercise considering the availability of sparsely-uniform well control in terms of ϕ_N and $\phi_D$log curves over the 3D seismic volume, we turned to a multiattribute regression approach to achieve our goal of obtaining ϕ_N and ϕ_D from seismic data. An optimal number of attributes along with operator length which exhibit the minimum validation error were selected for predicting the density and neutron porosities volume. The seismic attributes used in the neural networks are Poisson's ratio, E-rho, relative impedance, absolute P-impedance, S-impedance, and a filtered version of the input seismic data.

A representative crossplot from the predicted ϕ_D and ϕ_N volumes along an arbitrary line that passes through different wells are shown in Figure 6a. An equivalent crossplot from the well-log data is shown in Figure 6b. A striking similarity is seen between the two crossplots, which lends confidence in the approach that has been used. Further, using the Bayesian classification PDFs for each of the facies generated earlier, we generated the facies volume and their probability volume. A representative section through the facies volume passing through the different wells is shown in Figure 7. We notice straightaway that the carbonate content in Bone Spring increases as we go from the western to the eastern part of the line, which is as per our expectation and geological knowledge of the area. A clay-rich shale facies seen on the upper part of the Barnett, organic-rich shale seen on the lower portion of the Barnett, which might be prospective, and limy-shale and shaly-lime facies are seen in the interval from Wolfcamp to Barnett. In the Bone Spring interval, we notice a mix of tight limestone, calcareous mudstone and siliceous mudstone. The yellow color representing the siliceous mudstone seen on the western side of Wolfcamp is probably the production zone being tapped at the present time. To gain confidence in the facies analysis described thus far, we sought the available mud-log data for the other wells on the 3D seismic volume. We overlay the lithostrips obtained for two of the wells over this section. Notice the one-to-one correlation between the shale noticed in the Barnett, Wolfcamp units and more calcareous and siliceous mudstone with tight limestone in the Bone Spring interval. The presence of siliceous mudstone in the Wolfcamp unit on the well to the west correlates well with the prospective zone (green arrow) we interpreted based on the seismic facies analysis. Similarly, we notice more carbonate in the Bone Spring (light blue arrow) in the well to the east. The presence of shaly-lime (with more carbonate content) and limy-shale (little carbonate) correlates well with the mud-log lithostrip indicated with magenta and orange arrows. Such correlation between the seismic facies and the independent information coming from the mud-log records lends confidence in the analysis carried out. The probability volume also showed good corroboration.

Conclusions

We have tried to highlight the uncertainties in the estimation of volume of shale, water saturation and porosity from well-log data for unconventional reservoirs. In view of these uncertainties, we suggest that any deterministic approach for characterization of the target formations may not be appropriate and that a robust statistical approach should be adopted. For doing so we first demonstrate the interpretation of different types of lithofacies that could be carried out on a crossplot of $\phi_D$against ϕ_N from well log data and take it forward to execute a Bayesian classification approach using cut off values of $\phi_D$and ϕ_N for different facies in the broad zone of interest from Bone Spring to Mississippian. Once the $\phi_D$and ϕ_N attributes were determined from seismic data with the help of neutral networks, seismic lithofacies volume was generated which showed good correlation with the lithofacies interpretation carried out on mud log data. Such a robust statistical approach holds promise for its application in unconventional plays.

Acknowledgements

We wish to thank TGS for encouraging this work and for the permission to present and publish it. The well data used in this work was obtained from the TGS Well Data Library and is gratefully acknowledged.

10.1190/segam2019-3214084.1

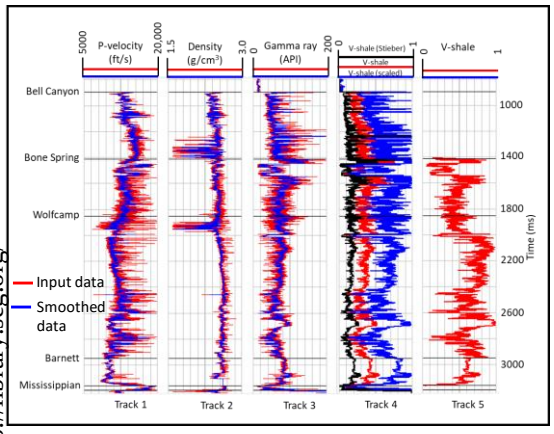

Figure 1: The sonic, density and gamma ray curves from a well in the Delaware Basin are shown in tracks 1, 2 and 3. The volume of shale curves corrected using scaling and Stieber corrections are shown in track 4. The volume of shale was computed by a petrophysicist by first subdividing the curves into three basic zones, namely the Bone Spring, Wolfcamp and the Barnett/Mississippian and the computations of gamma ray index were merged into a single composite curve, shown in track 5.

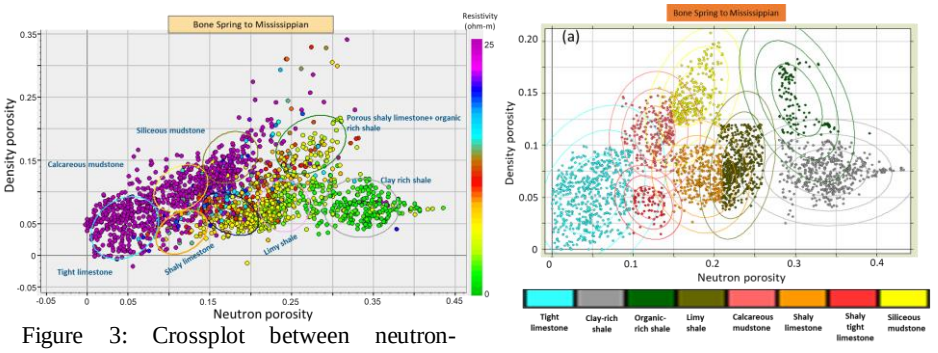

Figure 3: Crossplot between neutron-porosity and density-porosity for the litho-interval Bone Springs to Mississippian. The data points are coloured based on the resistivity values. Based on the information gathered so far, we assign the nomenclature to the cluster points as shown.

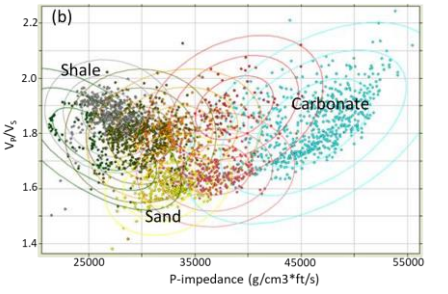

Figure 5: (a) Crossplot of P-impedance vs V_P/V_S, showing that it would be easy to distinguish between different lithologies (carbonate, sand and shale), but may be difficult to differentiate between shale characteristics, which might be useful for well completion processes. (b) Interpretation of litho-classification based on well log neutron and density porosity by restricting their values. The probability density functions for the individual clusters are also shown overlaid.

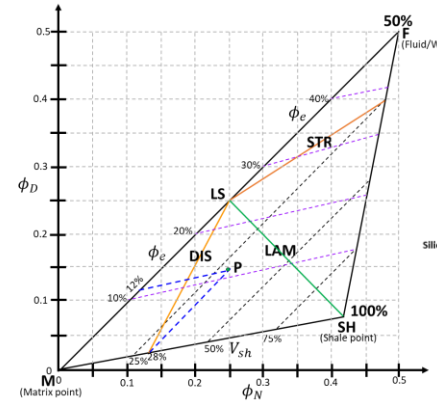

Figure 2: Crossplot between ϕ_N and ϕ_D for the formation interval of interest. The triangle shown between the shale point, matrix point and the fluid/water point can be used estimating the type of shale, volume of shale and effective porosity in the interval of interest.

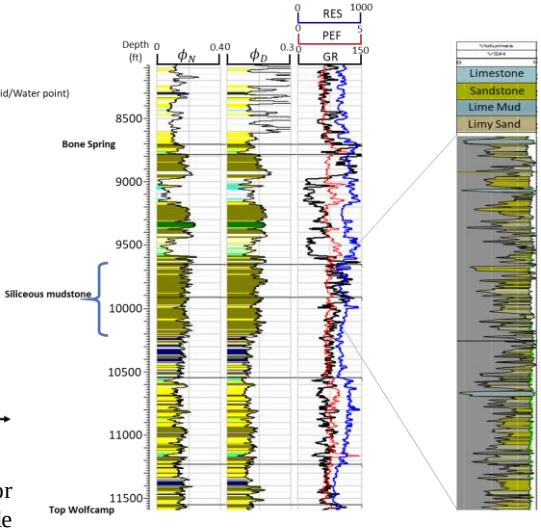

Figure 4: Interpretation of litho-column (siliceous mudstone) for well W1 based on the litho-classification carried out as shown in Figure 3.

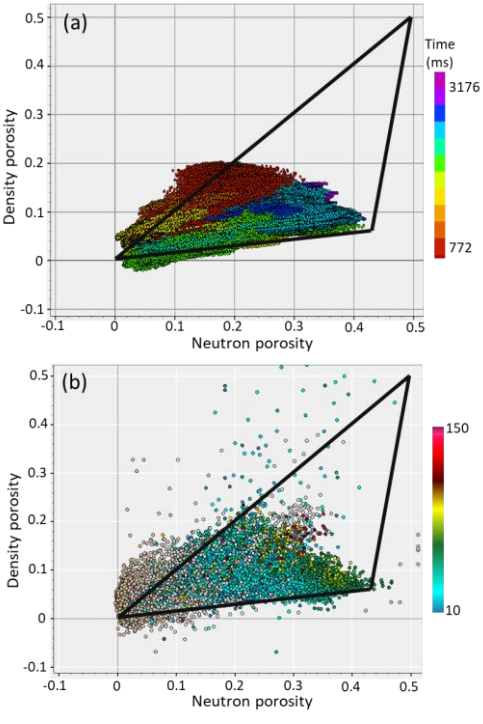

Figure 6: Equivalent crossplots of neutron-porosity and density porosity for the Bone Springs to Woodford shale interval from (a) seismically-derived data, and (b) well data.

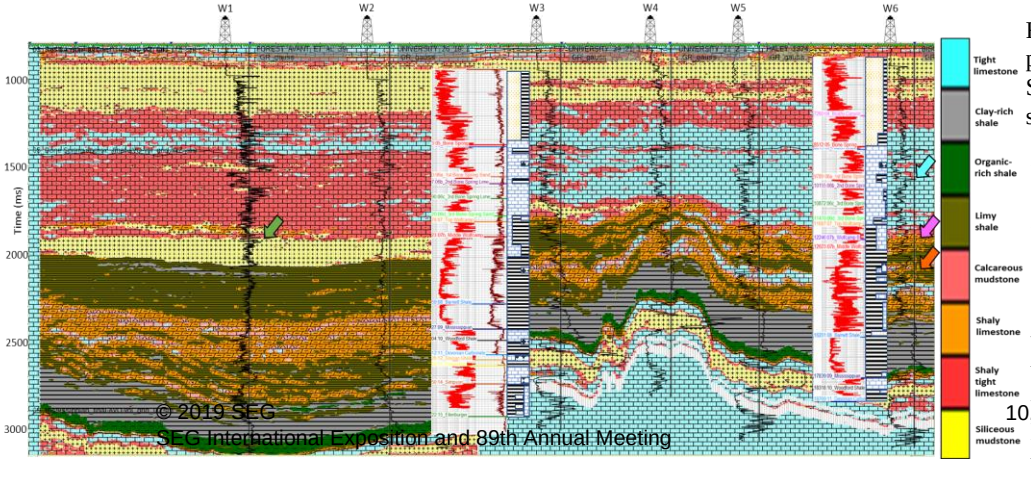

Figure 7: An arbitrary line passing through six different wells extracted through the facies volume. The gamma ray curves are overlaid on the display. The lithostrips obtained for two wells are overlaid on the display. One-to-one correlation is noticed between the shale in the Barnett and Wolfcamp and more sand and limestone in the Bone Spring interval. Also, more limestone content is noticed towards the right, which is closer to the Central Basin Platform. *(Data courtesy: TGS, Houston)*

10.1190/segam2019-3214084.1

REFERENCES

Alaskari, G. M. K., and A., Roozmeh, 2017, Determination of shale types using well logs: International Journal of Petrochemical Science and Engineering, **2**, 574–280, doi: https://doi.org/10.15406/ipcse.2017.02.00051.

Archie, G. E., 1952, Classification of carbonate reservoir rocks and petrophysical considerations: AAPG Bulletin, **36**, 218–298, doi: https://doi.org/10.1306/3D9343F7-16B1-11D7-8645000102C1865D.

Asquith, G., and D., Krygowski, 2004, Basic well log analysis: AAPG, AAPG Methods in Exploration Series 16, 31–35.

Clavier, C., W. R., Hoyle, and D., Meunier, 1971, Quantitative interpretation of thermal neutron decay time logs, Part-1. Fundamentals and techniques: Journal of Petroleum Technology, **23**, 743–755, doi: https://doi.org/10.2118/2658-A-PA.

Franseen, E. K., D., Stolz, and R. H., Goldstein, 2016, Available at https://doi.org/https://www.pbs-sepm.org/wp- content/uploads/2016/01/160119_Franseen_PBS-SEPM-Avalon-Talk-.pdf, accessed 1 November 2018.

Ghorab, M., M. A. M., Ramadan, and A. Z., Nouh, 2008, Australisn journal of Basic and Applied Sciences, **2**, 360–371.

Kim, T., S., Hwang, and S., Jang, 2016, Petrophysical approach for estimating porosity, clay volume, and water saturation in gas-bearing shale: A case study from the Horn River Basin, Canada: Austrian Journal of Earth Sciences, **109**, 289–298, doi: https://doi.org/10.17738/ajes.2016.0022.

Larinov, V. V., 1969, Borehole radiometry: Nedra.

Malik, M, C., Schmidt, E., Stockhausen, N. K., Vrubel, and K., Schwartz, 2013, Integrated petrophysical evaluation of unconventional reservoirs in the Delaware Basin: SPE Annual Technical Conference and Exhibition, SPE 166264, 1–19, doi: https://doi.org/10.2118/166264-MS.

Sharma, R. K., S., Chopra, J., Keay, H., Nemati, and L., Lines, 2018, Seismic reservoir characterization of Utica-Point Pleasant shale with efforts at fracability evaluation– Part 2: A case study: Interpretation, **6**, no. 2, T325–T336, doi: https://doi.org/10.1190/INT-2017-0135.1.

Steiber, S. J., 1970, Pulse-neutron capture log evaluation in the Louisiana Gulf Coast: 45th Annual Meeting, SPE, SPE-2961-MS, doi: https://doi.org/10.2118/2961-MS.

Simandoux, P., 1963, Dielectric measurements on porous media application to themeasurement of water saturations: study of the behaviour of argillaceous formations: Revue de l'Institut Francais du Petrole, **18**, Supplementary Issue, 193–215.